Temporal Instanton Analysis: Development and Implementation

Jonas A. Kersulis, *Student Member, IEEE,* and Ian A. Hiskens, *Fellow, IEEE*

***Abstract*—A previously-developed method for studying a transmission network's vulnerability to wind forecast inaccuracy is expanded. The method uses optimization to find a likely wind generation pattern that brings a specified line to an unacceptably high temperature. The objective quantifies wind pattern likelihood in terms of distance from the forecast, respecting spatial and temporal correlation between wind sites and time intervals. The set of constraints enforces power balance and ensures a chosen line in the network reaches a fixed temperature by the final time step. The thermal constraint is second-order in voltage angle differences, and is based on a DC-approximate line loss formulation. Repeatedly solving the QCQP for all lines in the network yields a set of instanton candidate generation patterns, which may then be sorted by likelihood. Having described the temporal instanton QCQP and its solution, the paper turns to a discussion of implementation details. Finally, a series of numerical experiments is presented. These experiments demonstrate the effect of an instanton pattern on line temperature trajectory, the effects of wind covariance on instanton analysis, and algorithm scaling properties.**

***Index Terms*—forecast uncertainty, optimization, transmission operations, wind energy**

I. Introduction

A WIND forecast error that was once inconsequential is now vexatious. As wind grows into a major transmission-scale energy source, system operators find themselves frequently dealing with wind-induced network congestion [1]. Operators use wind forecast data to steer the network, but wind forecasts are significantly less accurate than generation and demand predictions [2]. Might forecast deviations compound across a collection of wind farms to overheat a transmission line? Which lines are most vulnerable to such an event? Temporal instanton analysis addresses these questions by identifying sag-inducing wind patterns and ranking them according to likelihood. The intersection of likely wind patterns with those that cause excessive line heating is of interest to system operators and planners, who may use this information to better prepare for renewable generation uncertainty.

Instanton analysis belongs to the family of distance to failure algorithms. It was introduced in [3] and [4], where the DC power flow approximation was used to represent a network's feasible operating region as a set of linear constraints. These constraints form the faces of a high-dimensional polytope that contains all feasible network states. Distance to failure is intuitively understood to be the shortest distance between an operating point and the surface of the constraint polytope. As shown in [4], one can use convex optimization to quickly find the smallest shift in wind generation that will drive the network to a chosen polytope face. Once every face has been considered, the collection of shifts may be sorted by distance from the forecast operating point. The wind pattern corresponding to the shortest distance between the forecast operating point and the boundary of the constraint polytope is termed the instanton; it is the smallest shift in wind generation that will drive the network to the brink of infeasibility.

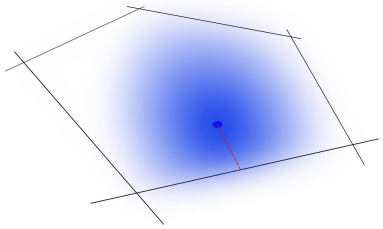

Fig. 1. How far is the forecast operating point from the edge of the feasible region, and might forecast inaccuracies drive the system there?

Instanton analysis research falls into two categories. The first is exploration of the trade-off between accuracy and algorithm complexity. Replacing the DC power flow approximation with the full AC model, for instance, yields greater accuracy at the cost of convexity [5]. Between the DC and AC extremes are various power flow approximations (see [6]–[8] for examples) which may be used to enhance accuracy while maintaining the solution guarantees of convexity. Regardless of the power flow model used, research in this category is ultimately focused on instantaneous vulnerability: find the smallest wind generation shift that drives a line to its steady-state power or current limit. This method uncovers previously hidden grid vulnerability, but it is safe to briefly operate a line above its current limit. As long as the line is allowed to cool before sagging to some limit (defined by statute and nearby trees), no harm is done. System operators know this; they periodically allow lines to operate above their rated steady-state limits to promote smooth operation during congestion [9]. Thus, if an operator is comfortable with temporarily overloaded lines, information from instantaneous instanton analysis may be too conservative to aid decision making. Temporal instanton analysis, the second research category, seeks to overcome this limitation by accommodating multiple time steps.

In this paper we expound on the temporal instanton analysis method introduced in [10]. By modeling line temperature over an appropriate time horizon, the proposed method discovers

The authors are with the Department of Electrical Engineering and Computer Science, University of Michigan, Ann Arbor, MI 48104 USA (e-mail: kersulis@umich.edu; hiskens@umich.edu)

This work was supported by the Los Alamos National Laboratory Grid Science Program, subcontract 270958.

multiple-time-step wind patterns that are both likely to occur and sure to bring at least one line in the network to its temperature limit. The remainder of this paper is organized as follows. Section II describes the models at the core of temporal instanton analysis. Section III combines these models into a quadratically-constrained quadratic program (QCQP). The solution of this QCQP is described in Section IV. Section V contains results for two networks: a modified version of the RTS-96 and the larger WECC network. The former network has been used in previous instanton analysis studies, while the latter serves to demonstrate scalability of temporal instanton analysis. Finally, an appendix contains a detailed description of the thermal model used to calculate line temperature.

We expand on prior work by providing a more detailed treatment of the objective function, discussing implementation details including computational complexity and sparsity, and proposing a particular algorithm for solving the secular equation.

II. Models

Temporal instanton analysis entwines three physical phenomena, each requiring a model. Transmission line temperature is based on a heat balance model, forecast error likelihood is quantified via a statistical model, and the feasible region of network operation is delineated using a network model. This section describes the three models in detail. The next section combines them into a quadratically-constrained quadratic program. Temporal instanton analysis consists of solving this QCQP for each line in a network.

A. Transmission Line Heating

A simplified relationship between power flow and line temperature is key to making temporal instanton analysis tractable. Starting with an IEEE standard [11], we derive an approximate recursive relationship between a line's temperature at one time step and voltage angle differences at all previous time steps. This relation is summarized below (and the Appendix contains a detailed derivation).

Consider a time horizon with n intervals, each on the order of ten minutes long. Power flow data is updated once per interval, but all other parameters (resistance, solar heating, etc.) remain constant. Choose a single transmission line in the network —suppose it lies between nodes i and j— and let this line's thermal limit be represented by $T_{\text{lim,C}}$ (°C). We can constrain the line's temperature at the end of the T-th interval to be equal to this limiting value by enforcing the second-order constraint

$$\sum_{k=1}^{n} \hat{\theta}_{ij}(t_k)^2 = \frac{a}{c}\left(T_{\text{lim,C}} - f\right), \tag{1}$$

where

$$\hat{\theta}_{ij}(t_k) = \theta_{ij}(t_k)\sqrt{(e^{a\bar{t}})^{n-k+1} - (e^{a\bar{t}})^{n-k}} \tag{2a}$$

$$a = \frac{1}{mC_p}\left[-\eta_c - 4\eta_r T_{\text{m,K}}^3\right] \tag{2b}$$

$$c = \frac{r_{ij} S_b}{3mC_p x_{ij}^2 L_{ij}} \tag{2c}$$

$$d = \frac{\eta_c T_{\text{a,C}} + \eta_r\left(4T_{\text{m,C}}T_{\text{m,K}}^3 + T_{\text{a,K}}^4 - T_{\text{m,K}}^4\right) + q_s}{mC_p} \tag{2d}$$

$$f = (e^{a\bar{t}})^n T_{\text{l,C}}^0 + \frac{d}{a}\left[\sum_{i=1}^{n}\left((e^{a\bar{t}})^i - (e^{a\bar{t}})^{i-1}\right)\right] \tag{2e}$$

In (2a), $\theta_{ij}(t_k)$ is the angle difference across line $i-j$ at time interval t_k, and $\bar{t}$ is the length of each time interval (in seconds). In (2b), a is a constant with units of s^{-1}; mC_p is the heat capacity in J/m-°C; η_c is the conductive heat loss rate coefficient in W/m-°C; η_r is the conductive heat loss rate coefficient in W/m-°C^4; and $T_{\text{m,K}}$ is the average of ambient temperature $T_{\text{a,K}}$ and limit temperature $T_{\text{lim,K}}$, in Kelvin. In (2c), c is a constant with units of W/m; r_{ij} and x_{ij} are the resistance and reactance of line $i-j$ in per unit, respectively; S_b is the system base (e.g. 100 MVA); and L_{ij} is the length of one phase of line $i-j$ conductor, in meters. In (2d), d is a constant with units of W/m, and q_s is the solar heat gain rate in W/m. Finally, in (2e), f is a constant with units of degrees Celsius, and $T_{\text{l,C}}^0 = T_{\text{l,C}}(t_0)$ is the line's initial temperature (based on generator dispatch and forecast) in Celsius.

This line temperature constraint model rests on a DC line loss approximation from [12]; see the Appendix for details.

B. Wind Forecast Inaccuracy

Correlation must be considered when modeling forecast deviations for a collection of wind farms. Distance from the forecast tends to be a good proxy for a particular deviation pattern's likelihood,[1] but wind behavior is somewhat more complex. Consider several wind farms scattered across a transmission grid, each with a forecast power output. Let the error in this forecast be represented by a zero-mean Gaussian random variable.[2] Then the wind forecast deviation pattern for a single time step takes takes the form of a Gaussian random vector. Elements of this vector are correlated due to spatial relationships between wind sites: if wind speed increases at one site, for instance, a simultaneous decrease at a neighboring site is unlikely. In addition to spatial correlation, there may also be temporal relationships between wind farms. Increased wind speed at one site during the current time interval may be correlated with greater wind speed at downwind sites during the following interval, for example.

Suppose a network has N_R wind sites and we wish to consider n time intervals. Let $\mathbf{r}$ be the $(N_R \cdot n) \times 1$ vector of forecast deviations across all wind sites and time intervals. The first n elements of $\mathbf{r}$ contain forecast errors for the first

[1]For independent power injections like conventional generators or demand nodes, this intuitive model may be adequate.

[2]For time scales shorter than roughly one hour, a Cauchy distribution is more appropriate, but forecast errors are commonly assumed to be Gaussian nonetheless. See [13].

site at time intervals 1 to n, the second n elements are errors for the second site, and so on. The probability density function for $\mathbf{r}$ is

$$f(\mathbf{r}) = \frac{\exp\left(-\frac{1}{2}\mathbf{r}^\top \mathbf{C}^{-1}\mathbf{r}\right)}{(2\pi)^{\frac{n}{2}}\sqrt{\det \mathbf{C}}}\ , \tag{3}$$

where $\mathbf{C}$ is the correlation matrix. Maximizing f corresponds to minimizing $\mathbf{r}^\top \mathbf{C}^{-1}\mathbf{r}$. Thus, one may express a desire to maximize wind pattern likelihood with

$$\min\ \mathbf{r}^\top \mathbf{Q}\mathbf{r}, \tag{4}$$

where $\mathbf{Q} = \mathbf{C}^{-1}$ is the precision matrix. There are many ways to determine $\mathbf{C}$ or $\mathbf{Q}$ from historical data. The authors of [14] use maximum likelihood optimization to fit a set of parameters to observed data, thereby generating a sparse precision matrix. Another option is to compute a sample correlation matrix from time series data.

C. Network Model

Undesirable scenarios found by temporal instanton analysis are of no consequence if they are infeasible. Our problem formulation must We use DC power flow to express the feasible region of operation as a set of linear constraints. [3] The other noteworthy detail of our power network model is distributed slack. The mismatch between total power generation and demand at any time step is divided over multiple generators according to a vector of participation factors. This slack model is more realistic than the single slack bus, which assumes one generator compensates for all mismatch. (Of course, there is still an angle reference bus θ_{ref}.)

The three models described in this section are sufficient to express temporal instanton analysis mathematically. The next section combines them into a QCQP.

III. Temporal Instanton QCQP

The following quadratically constrained quadratic program is a concise expression of our desire to find feasible, likely wind patterns that will cause one transmission line in the network to reach its temperature limit by the end of a certain time horizon:

$$\min_{\mathbf{r}} \quad \mathbf{r}^\top \mathbf{Q}\mathbf{r} \tag{5a}$$

subject to:

$$\sum_{k=1}^{n} \hat{\theta}_{ij}(t_k)^2 = \frac{a}{c}\left(T_{\text{lim,C}} - f\right) \ \text{ for some } (i,j) \in \mathcal{G} \tag{5b}$$

$$\sum_{j} Y_{ij}\theta_{ij,t_k} = G_{i,t_k} + (R_{i,t_k} + \mathbf{r}_{i,t_k}) - D_{i,t_k} \qquad \forall i \in 1...N,\ k \in 1...n \tag{5c}$$

$$\mathbf{G}_{t_k} = \mathbf{G}_{0,t_k} + \alpha_{t_k}\mathbf{g} \quad \forall k \in 1\dots n \tag{5d}$$

$$\theta_{ref,t_k} = 0 \qquad \forall k \in 1\dots n \tag{5e}$$

In (5), N represents the number of nodes in the network, n the number of time steps, and $\mathcal{G}$ the set of edges (transmission lines). The objective (5a) matches (4) and expresses a desire to find wind patterns that are likely to occur (see Section II-B). In this objective, $\mathbf{r}$ is the vector of wind output forecast errors, and $\mathbf{Q}$ is the precision (or inverse covariance) matrix. The first constraint (5b) forces the temperature of a particular line to reach $T_{\text{lim,C}}$ degrees Celsius at the final time t_n. (See Section II-A for a detailed explanation.) In (5c), which enforces DC power balance, Y_{ij} is the $[i,j]$-th element of the admittance matrix (which assumes zero resistance); θ_{ij,t_k} is the difference between voltage angles θ_i and θ_j at time t_k; G_{i,t_k} is conventional active power generation at node i and time t_k; $(R_{i,t_k} + \mathbf{r}_{i,t_k})$ is the sum of renewable generation forecast and forecast error for wind node i at time t_k (equal to zero if node i has no wind farm); and D_{i,t_k} is the power demand for bus i at time t_k. Constraint (5d) implements droop response: scheduled generation at time t_k is represented by the vector G_{0,t_k}, and each generator G_i compensates for of power mismatch α_{t_k} according to its participation factor $\mathbf{g}_i$. Finally, the constraint (5e) establishes the angle reference bus.

The mathematical program (5) has a quadratic objective function, a set of linear constraints, and a single quadratic constraint. We can emphasize this QCQP form by combining all variables into a single vector z and re-writing (5) as

$$\min \quad \mathbf{z}_1^\top \mathbf{Q}_{\text{obj}}\mathbf{z}_1 \tag{6a}$$

$$s.t. \quad \mathbf{z}_3^\top \mathbf{z}_3 = c \tag{6b}$$

$$\mathbf{A}\mathbf{z} = \mathbf{b}. \tag{6c}$$

The objective (6a) is equivalent to (5a), the quadratic equality constraint (6b) is equivalent to (5b), and the linear equality constraint (6c) combines (5c)-(5e). The vector $\mathbf{z}$ consists of $n \cdot (N + N_R + 2)$ variables, where n is the number of time steps, N is the number of nodes, and N_R is the number of nodes with wind generation. Subscripts are used to distinguish variable types: $\mathbf{z}_1 \in \mathbb{R}^{n \cdot N_R}$ contains all wind deviations $\mathbf{r}$, $\mathbf{z}_2 \in \mathbb{R}^{n\cdot(N+1)}$ contains angle and mismatch variables, and $\mathbf{z}_3 \in \mathbb{R}^n$ contains auxiliary angle difference variables involved in line temperature calculation (this is what permits the clean norm form of (6b)).

Solving (6) for each line in the network yields a set of instanton candidate wind patterns, each of which will heat a particular line to its thermal limit. Of these candidates, the one with lowest objective value is the instanton wind pattern. The next section contains a solution method for QCQPs of the form (6), based in part on work in [15].

IV. QCQP Solution Method

By now the difference between instantaneous and temporal analyses is clear. Instead of a quadratic program, whose solution readily obtained from KKT conditions, we have a QCQP. The root of this difference is the fact that one cannot express resistive losses—even approximately—as a linear constraint. QCQPs are NP-hard in general; solutions may exist, but unless the quadratic constraint matrices are positive-definite there is no solution guarantee [16]. Fortunately, our QCQP belongs to the family of trust region subproblems. As shown in [15], it may be solved in polynomial time. Our solution method, originally presented in [10], divides into four steps.

[3] These assumptions imply a flat voltage profile, negligible line resistance (though resistance values are used to calculate line temperatures), and linearity of the sine function.

A. Translation

The first step is to change variables from $\mathbf{z}$ to $\mathbf{y} = \mathbf{z} - \mathbf{z}^*$, where $\mathbf{z}^* \in \{\mathbf{z} : \mathbf{A}\mathbf{z} = \mathbf{b}\}$. This translation transforms $\mathbf{A}\mathbf{z} = \mathbf{b}$ into $\mathbf{A}\mathbf{y} = \mathbf{0}$. To prevent the change from introducing a linear term into the quadratic constraint, we require $\mathbf{z}_3^* = \mathbf{0}$. To satisfy $\mathbf{A}\mathbf{z}^* = \mathbf{b}$, the subvectors $\mathbf{z}_1^*$ and $\mathbf{z}_2^*$ must satisfy

$$\mathbf{A}\begin{bmatrix}\mathbf{z}_1^* \\ \mathbf{z}_2^* \\ \mathbf{0}\end{bmatrix} = \mathbf{b}.$$

It is straightforward to find a min-norm $\mathbf{z}^*$ that satisfies this constraint by partitioning and factorizing $\mathbf{A}$ appropriately. After translation, the problem becomes

$$\begin{aligned} \min \quad & \mathbf{y}_1^\top \mathbf{Q}_{\text{obj}}\mathbf{y}_1 + 2\mathbf{y}_1^\top \mathbf{Q}_{\text{obj}}\mathbf{z}_1^* && \text{(7a)} \\ s.t. \quad & \mathbf{y}_3^\top \mathbf{y}_3 = c && \text{(7b)} \\ & \mathbf{A}\mathbf{y} = \mathbf{0}. && \text{(7c)} \end{aligned}$$

B. Kernel mapping

The form of (7c) suggests an intuitive explanation: any solution to (7) must lie in the nullspace (kernel) of $\mathbf{A}$. If $\dim \mathcal{N}(\mathbf{A}) = n$ is the dimension of this nullspace, we can let $\mathbf{y} = \mathbf{N}\mathbf{x}$ where the n columns of $\mathbf{N}$ span $\mathcal{N}(\mathbf{A})$. This change of variables is akin to a rotation, but reduces the problem dimension to n. Partitioning $\mathbf{N}$ according to,

$$\begin{bmatrix}\mathbf{y}_1 \\ \mathbf{y}_2 \\ \mathbf{y}_3\end{bmatrix} = \begin{bmatrix}\mathbf{N}_1 \\ \mathbf{N}_2 \\ \mathbf{N}_3\end{bmatrix}\mathbf{x}$$

allows (7) to be written,

$$\begin{aligned} \min \quad & \mathbf{x}^\top(\mathbf{N}_1^\top \mathbf{Q}_{\text{obj}}\mathbf{N}_1)\mathbf{x} + 2\mathbf{x}^\top(\mathbf{N}_1^\top \mathbf{Q}_{\text{obj}}\mathbf{z}_1^*) && \text{(8a)} \\ s.t. \quad & \mathbf{x}^\top \mathbf{N}_3^\top \mathbf{N}_3 \mathbf{x} = c. && \text{(8b)} \end{aligned}$$

All feasible solutions to (8) lie in the nullspace of A, so the linear constraints are rendered implicit.

C. Obtaining a norm constraint

After kernel mapping, the quadratic constraint is no longer a norm constraint. This can be corrected in two steps. First, perform an eigendecomposition $\mathbf{N}_3^\top \mathbf{N}_3 = \mathbf{U}\mathbf{D}\mathbf{U}^\top$ and let $\hat{\mathbf{x}} = \mathbf{U}^\top \mathbf{x}$. The constraint is diagonal in terms of $\hat{\mathbf{x}}$:

$$\mathbf{x}^\top \mathbf{N}_3^\top \mathbf{N}_3 \mathbf{x} = \hat{\mathbf{x}}^\top \mathbf{D} \hat{\mathbf{x}} \tag{9}$$

where $\mathbf{D}$ is diagonal and has at most n nonzero elements. The right side of (9) may be expanded into:

$$\begin{bmatrix}\hat{\mathbf{x}}_1^\top & \hat{\mathbf{x}}_2^\top\end{bmatrix}\begin{bmatrix}\mathbf{0} & \mathbf{0} \\ \mathbf{0} & \hat{\mathbf{D}}\end{bmatrix}\begin{bmatrix}\hat{\mathbf{x}}_1 \\ \hat{\mathbf{x}}_2\end{bmatrix}. \tag{10}$$

The second step is to change variables from $\hat{\mathbf{x}}$ to $\mathbf{w} = [\mathbf{w}_1^\top \ \mathbf{w}_2^\top]^\top$. The variables $\mathbf{x}$, $\hat{\mathbf{x}}$, and $\mathbf{w}$ are related through:

$$\begin{aligned} \begin{bmatrix}\mathbf{w}_1 \\ \mathbf{w}_2\end{bmatrix} &= \begin{bmatrix}\mathbf{I} & \mathbf{0} \\ \mathbf{0} & \hat{\mathbf{D}}^{1/2}\end{bmatrix}\begin{bmatrix}\hat{\mathbf{x}}_1 \\ \hat{\mathbf{x}}_2\end{bmatrix} = \mathbf{K}\hat{\mathbf{x}} && \text{(11)} \\ \implies \mathbf{w} &= \mathbf{K}\mathbf{U}^\top \mathbf{x}. \end{aligned}$$

(Note that $\mathbf{x} = \mathbf{U}\mathbf{K}^{-1}\mathbf{w}$ because $\mathbf{U}\mathbf{U}^\top = \mathbf{I}$.) In terms of $\mathbf{w}$, (8b) is transformed through (9) to give the form of a norm:

$$\hat{\mathbf{x}}^\top \mathbf{D}\hat{\mathbf{x}} = \hat{\mathbf{x}}_2^\top \hat{\mathbf{D}}^{1/2}\hat{\mathbf{D}}^{1/2}\hat{\mathbf{x}}_2 = \mathbf{w}_2^\top \mathbf{w}_2 \ . \tag{12}$$

Of course, this change of variables must also be applied to the cost function. After substitution and simplification, the full problem becomes:

$$\begin{aligned} \min \quad & \mathbf{w}^\top \mathbf{B}\mathbf{w} + \mathbf{w}^\top \mathbf{b} && \text{(13a)} \\ s.t. \quad & \mathbf{w}_2^\top \mathbf{w}_2 = c && \text{(13b)} \end{aligned}$$

where

$$\begin{aligned} \mathbf{B} &= \mathbf{K}^{-1}\mathbf{U}^\top \mathbf{N}_1^\top \mathbf{Q}_{\text{obj}}\mathbf{N}_1 \mathbf{U}\mathbf{K}^{-1} \\ \mathbf{b} &= 2\mathbf{K}^{-1}\mathbf{U}^\top \mathbf{N}_1^\top \mathbf{Q}_{\text{obj}}\mathbf{z}_1^* \end{aligned}$$

The manipulations in this section have restored the norm structure of the quadratic constraint. In the next section we use the KKT conditions of (13) to eliminate $\mathbf{w}_1$, the unconstrained part of $\mathbf{w}$. This will allow us to write the objective in terms of $\mathbf{w}_2$ only.

D. Eliminating $\mathbf{w}_1$

Note that $\mathbf{w}_1$ is unconstrained in (13). For a fixed $\mathbf{w}_2$, we can use the KKT conditions to find $\mathbf{w}_1$ such that the objective is minimized. Begin by expanding the objective:

$$\begin{aligned} f(\mathbf{w}) &= \begin{bmatrix}\mathbf{w}_1^\top & \mathbf{w}_2^\top\end{bmatrix}\begin{bmatrix}\mathbf{B}_{11} & \mathbf{B}_{12} \\ \mathbf{B}_{12}^\top & \mathbf{B}_{22}\end{bmatrix}\begin{bmatrix}\mathbf{w}_1 \\ \mathbf{w}_2\end{bmatrix} + \begin{bmatrix}\mathbf{w}_1^\top & \mathbf{w}_2^\top\end{bmatrix}\begin{bmatrix}\mathbf{b}_1 \\ \mathbf{b}_2\end{bmatrix} \\ &= \mathbf{w}_1^\top \mathbf{B}_{11}\mathbf{w}_1 + 2\mathbf{w}_1^\top \mathbf{B}_{12}\mathbf{w}_2 + \mathbf{w}_2^\top \mathbf{B}_{22}\mathbf{w}_2 \\ &\quad + \mathbf{w}_1^\top \mathbf{b}_1 + \mathbf{w}_2^\top \mathbf{b}_2. \end{aligned}$$

Next, set the partial derivative with respect to $\mathbf{w}_1$ equal to zero:

$$\begin{aligned} \frac{\partial f}{\partial \mathbf{w}_1} &= 2\mathbf{w}_1^\top \mathbf{B}_{11} + 2\mathbf{w}_2^\top \mathbf{B}_{12}^\top + \mathbf{b}_1^\top = \mathbf{0} \\ \implies \mathbf{w}_1 &= -\mathbf{B}_{11}^{-1}\left(\mathbf{B}_{12}\mathbf{w}_2 + \frac{1}{2}\mathbf{b}_1\right). \end{aligned} \tag{14}$$

After substitution of (14), the objective depends only on $\mathbf{w}_2$:

$$\begin{aligned} f(\mathbf{w}_2) = \mathbf{w}_2^\top &\left(\mathbf{B}_{22} - \mathbf{B}_{12}^\top \mathbf{B}_{11}^{-1}\mathbf{B}_{12}\right)\mathbf{w}_2 \\ &+ \mathbf{w}_2^\top(\mathbf{b}_2 - \mathbf{B}_{12}^\top \mathbf{B}_{11}^{-1}\mathbf{b}_1). \end{aligned}$$

(Note that the constant term, which plays no role in minimization, was omitted.) The full optimization problem becomes:

$$\begin{aligned} \min \quad & \mathbf{w}_2^\top \hat{\mathbf{B}}\mathbf{w}_2 + \mathbf{w}_2^\top \hat{\mathbf{b}} && \text{(15a)} \\ s.t. \quad & \mathbf{w}_2^\top \mathbf{w}_2 = c, && \text{(15b)} \end{aligned}$$

where

$$\begin{aligned} \hat{\mathbf{B}} &= \mathbf{B}_{22} - \mathbf{B}_{12}^\top \mathbf{B}_{11}^{-1}\mathbf{B}_{12} \\ \hat{\mathbf{b}} &= \mathbf{b}_2 - \mathbf{B}_{12}^\top \mathbf{B}_{11}^{-1}\mathbf{b}_1. \end{aligned}$$

This is a QCQP in n dimensions with a single norm constraint. It is straightforward to obtain solutions to this problem, as the next subsection shows.

E. Solution via Enumeration

A straightforward method of solving (15) involves initially diagonalizing $\hat{\mathbf{B}}$ through an eigendecomposition. It will be assumed that step has been completed. Let v be the Lagrange multiplier associated with (15b) and write the first-order optimality condition for (15):

$$\frac{\partial \mathcal{L}(\mathbf{w}_2, v)}{\partial \mathbf{w}_2} = 2\hat{\mathbf{B}}\mathbf{w}_2 + \hat{\mathbf{b}} - v(2\mathbf{w}_2) = 0$$
$$\implies \hat{\mathbf{B}}\mathbf{w}_2 + \hat{\mathbf{b}}/2 = v\mathbf{w}_2 \ . \tag{16}$$

Equation (16) is a linear system that yields $\mathbf{w}_2$ for fixed v:

$$\mathbf{w}_{2,i} = \frac{\hat{\mathbf{b}}_i/2}{v - \hat{\mathbf{B}}_{i,i}} \ . \tag{17}$$

In addition to satisfying (17), an optimal $\mathbf{w}_2$ must satisfy (15b). Substituting (17) into the latter yields the secular equation:

$$s(v) = \sum_i \left(\frac{\hat{\mathbf{b}}_i/2}{v - \hat{\mathbf{B}}_{i,i}} \right)^2 = c \tag{18}$$

Note that $s(v)$ has one pole per unique nonzero diagonal element of $\hat{\mathbf{B}}$. There are at most two solutions per pole, one on each side. This is best understood graphically. Figure 2 illustrates a three-pole secular equation taken from analysis of the RTS-96 network. The Lagrange multiplier v is on the horizontal axis, and the secular equation value $s(v)$ is on the vertical. Solutions are intersections of $s(v)$ with the horizontal line $s(v) = c$. They can be computed numerically with a simple binary search algorithm.

V. Implementation

Temporal instanton analysis consists of solving a Section III QCQP via the Section IV method for each line in the network. Each QCQP instance is independent from, and nearly identical to, all others. (Only rows of $\mathbf{A}$ corresponding to scaled angle differences change as one line is replaced by another.) Computation and storage requirements for a single QCQP instance depend on network size, and total processing time is directly proportional to the number of lines in the network. Provided one has as many computing cores as there are lines in the network, solution time may be reduced to that of a single QCQP plus initialization and memory sharing overhead. For machines with only a few cores (like the four-core laptop we used), careful implementation is required to make the method scale well.[4] We call attention to three important implementation considerations.

A. Sparsity

Sparsity is of the utmost importance in temporal instanton analysis. Because each piece of (6) is dominated by zeros, sparsity plays a key role in matrix building before any algebraic manipulations are performed. The objective, for example, contains only a subset $\mathbf{z}_1$ of the variables; portions of $\mathbf{Q}_{\text{obj}}$ corresponding to $\mathbf{z}_2$ and $\mathbf{z}_3$ consist entirely of zeros. Even the nonzero portion of $\mathbf{Q}_{\text{obj}}$ (the precision matrix $\mathbf{Q}$) is sparse if the method of [14] is used to generate it. The constraints (6b) and (6c) are similarly sparse.[5] Of course, the benefits of sparsity also apply to operations like concatenation, multiplication, and factorization.

B. Factorization

Matrix factorization, a relatively expensive operation, occurs three times in the Section IV solution method. First, a portion of the $\mathbf{A}$ matrix must be factorized to determine the translation point $\mathbf{z}^*$. A sparse method should be used here to ease the computational burden. A second factorization is necessary to construct a basis for the kernel of $\mathbf{A}$. Here a sparse QR factorization routine may be used.[6] The third factorization is an eigendecomposition, as described in Section IV-C. This step is a bottleneck, owing to the fact that $\mathbf{N}_3$ in (9) is dense.

C. Secular Equation

Solutions to the secular equation are intersections between the curve defined in (18) and a horizontal line (see Figure 2). The number of solutions varies from 2 to $2n$ (n being the number of time steps) with the value of c. Empirical study shows that numerator and pole values range from 10^2 to 10^8 and higher, depending on the number, size, and placement of wind farms, and the overall size of the network. (The constant c, by contrast, is always small, typically on the order of 10^{-2}.) It is nontrivial to write a secular equation solver capable of efficiently handling this variety of parameter values. Our solver times out when numerator values are extremely high; though there are technically at least two solutions to the secular equation, values of v corresponding to these solutions translate to physically impossible, or even absurd, wind power variations (e.g. 100 GW for a 20 MW wind farm).

VI. Results

We performed numerical experimentation with three goals in mind. The first is to illustrate the relationship between the instanton pattern and a line's temperature trajectory. How does line temperature evolve in response to instanton angle differences? Second, numerical experimentation can illustrate the effects of wind covariance. What impact does a reasonable covariance matrix have on instanton objective values and wind patterns? The third goal is to characterize algorithm scaling. What is the relationship between the number of wind farms (decision variables) and algorithm performance? How does the solution time of a single QCQP vary with network size and topology?

In every numerical experiment we assumed Waxwing conductors, considered six time steps, and gradually increased the wind forecast over time while keeping conventional generation and demand constant.

[4] The relationship between number of workers and overall performance is not necessarily intuitive. On our four-core laptop, two workers were able to cut overall computation time in half with a modest increase in memory allocation. When we used four worker processes, however, the savings were eclipsed by communication and data sharing costs.

[5] A dense matrix representation of (6b) for the RTS-96 network with six time steps occupies 2.5 megabytes dense; a sparse version takes just 40 bytes.

[6] The SPQR algorithm in SuiteSparse [17] is well suited.

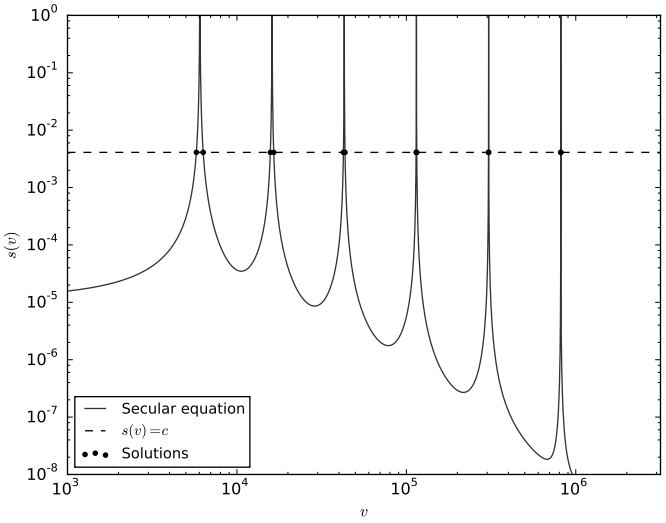

Fig. 2. Secular equation for a single line (corresponding to the instanton) in the RTS-96. Because there were six time steps in the analysis, $s(v)$ approaches infinity at six poles. Dots show the six solutions to $s(v) = c$ identified by our secular equation solver. Note that there could be as few as two solutions if c were small enough.

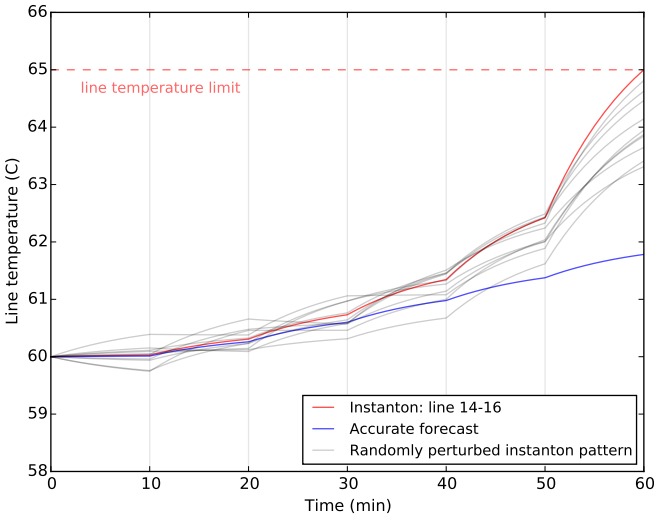

Fig. 3. RTS-96 temperature trajectories for the line between nodes 14 and 16. Red represents the instanton trajectory, which brings the line to its temperature limit of 65 C. Trajectories shown in gray arise from randomly perturbed versions of the instanton wind pattern having the same objective value. The blue trajectory corresponds to zero deviation from the wind forecast.

A. Temperature Trajectories

The modified RTS-96 network from [18] provides a helpful test case for illustrating instanton analysis. The network has eighteen wind farms distributed across three areas: nine in the first area, six in the second, and three in the third. Transmission lines are assumed to be Waxwing conductors, as in [19]. We assume all lines begin at 60 C and have temperature limits of 65 C. We performed instanton analysis for a one-hour time horizon divided into six ten-minute intervals. Figure 3 illustrates temperature trajectories corresponding to the instanton and nearby wind patterns. The instanton pattern causes the line to reach 65 C, but if we randomly perturb the instanton pattern while keeping the objective value constant, the line does not reach its temperature limit.

B. Effects of Covariance

To illustrate the effects of covariance on temporal instanton analysis, we used a simple heuristic method to generate a reasonable spatial covariance matrix for the RTS-96.[7]

Introducing a positive-definite, unit-norm covariance matrix allows the QCQP solution algorithm to find patterns with lower objective value. Figure 4 shows that these patterns have higher objective value when the original objective function (simple two-norm) is used.

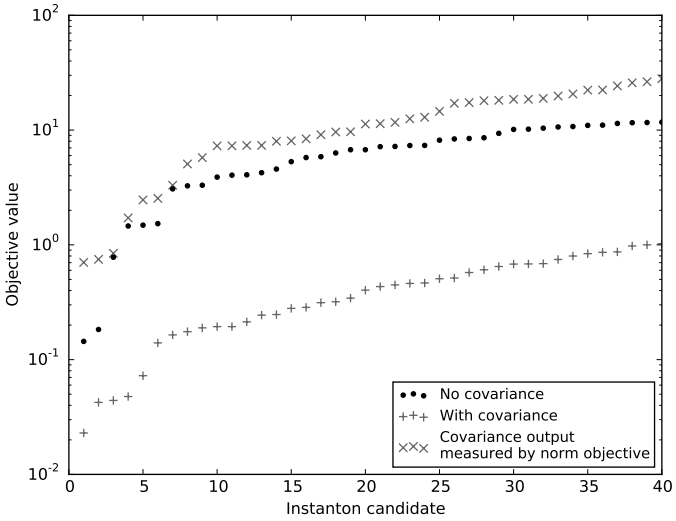

Fig. 4. Objective values for lowest forty instanton candidates, with and without covariance. "Covariance output measured by norm objective" was computed by passing solution vectors from the covariance analysis output to the objective function from the no-covariance case.

C. Algorithm Scaling

We performed two tests to characterize scaling of our algorithm. First, we varied the number of wind nodes in the RTS-96 network and, considering a time horizon of one hour divided into six equal time intervals, performed a complete analysis in each case. Figure 5 illustrates the relationship between QCQP size and the time required to perform a complete analysis. Second, we added wind farms to ten of the test cases packaged with MATPOWER [21] and analyzed each. For each network we chose to add a number of wind nodes equal to the number of conventional generators, placed the wind sites randomly, and sized each site to fix wind penetration at 50%. The choice of these parameters is somewhat arbitrary for the purposes of characterizing algorithm scaling, but we were careful to add enough significantly-sized wind farms to

[7]After assigning geographic coordinates to each of the eighteen wind farms and constructing a distance matrix, we mapped distances to correlation coefficients using a relationship from [20].

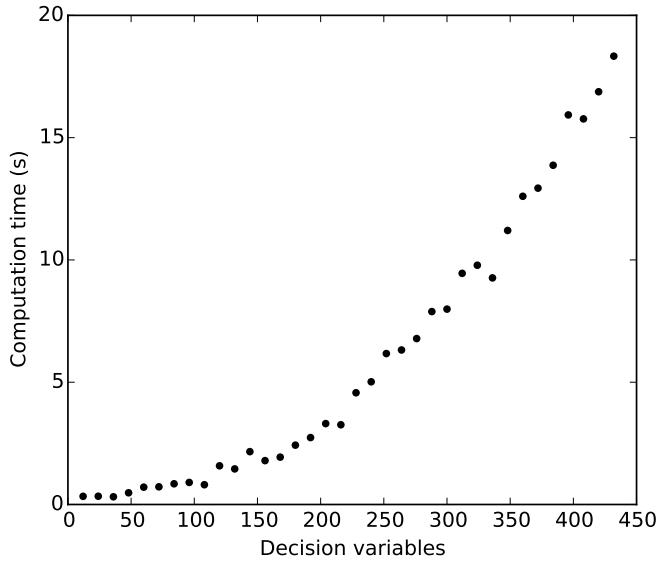

Fig. 5. Total computation time for 119 lines (QCQPs) as a function of total decision variables. The network is the RTS-96, and the time horizon is one hour divided into six ten-minute intervals. Starting with two, the number of wind farms was increased two at a time up to 72 (the network has 73 nodes), and these wind farms were randomly placed throughout the network.

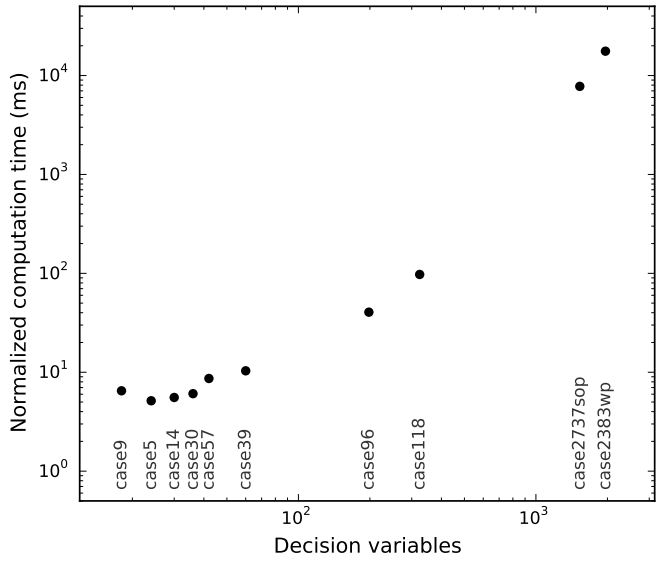

Fig. 6. Average computation time (total time divided by number of lines analyzed) for ten Matpower cases, on a log-log scale. For each network, the number of wind farms is equal to the number of conventional generators, and wind nodes were chosen randomly. In every case the time horizon is five minutes divided into six thirty-second intervals.

each network to avoid numerical difficulties.[8] Figure 6 shows average computation time for a single QCQP versus network size. As a reference point for overall solution time, it took just over two hours for our four-core laptop with 8 GB of RAM to analyze every line in the Polish summer 2008 peak network (case `3120sp` in Matpower).

[8]If there are too few wind nodes or penetration is too low, many solutions will have absurdly high objective value, and our routine will time out.

VII. Conclusion

This paper has extended the temporal instanton analysis method presented in [10] with a focus on implementation and algorithm scaling. A DC-approximate line loss expression allowed us to write a recursive relationship between a line's final and initial temperatures in terms of voltage angle differences during a sequence of discrete time steps.

Appendix
Line Temperature Model

A. Heat Balance Equation

The change in temperature of any object may be expressed as a differential equation called the heat balance equation, which relates temperature change to a sum of various sources of heating. The IEEE 738 standard [11] provides the following heat balance equation for a transmission line:

$$\frac{dT}{dt} = \frac{1}{m \cdot C_p} \left[I^2 \cdot R(T_{\mathrm{l,C}}(t)) - q_c - q_r + q_s \right] \tag{19}$$

In (19), $T_{\mathrm{l,C}}(t)$ is the conductor average temperature in Celsius, $m \cdot C_p$ is the product of mass and heat capacity, and $I^2 \cdot R(T_{\mathrm{l,C}}(t))$ represents heat rate due to resistive heating. q_c represents convective heat loss, which is proportional to the temperature difference between the line and surrounding air:

$$q_c = \eta_c \cdot (T_{\mathrm{l,C}}(t) - T_{\mathrm{a,C}}) \ , \tag{20}$$

where $T_{\mathrm{a,C}}$ is the ambient temperature in Celsius. q_r in (19) represents radiation heat loss, modeled by the fourth-order expression

$$q_r = \eta_r \cdot \left[T_{\mathrm{l,K}}(t)^4 - T_{\mathrm{a,K}}^4 \right] , \tag{21}$$

where $T_{\mathrm{l,K}}(t)$ and $T_{\mathrm{a,K}}$ are the conductor and ambient temperatures in Kelvin, respectively. Finally, q_s in (19) represents solar heating. In this paper q_s is fixed to some conservative constant (corresponding to full, direct sun).

B. DC Line Loss Approximation

We replace the resistive heat rate term $I^2 \cdot R(T_{\mathrm{l,C}}(t))$ by f_{ij}^{loss}, the approximate line loss expression derived in [12]:

$$f_{ij}^{\mathrm{loss}} \approx r_{ij} \left(\frac{\theta_{ij}}{x_{ij}} \right)^2 , \tag{22}$$

where θ_{ij} is the difference between angles θ_i and θ_k, and $r_{ij} + jx_{ij}$ is the impedance of the line between nodes i and j. Three DC power flow assumptions underpin (22): voltage magnitudes are all 1pu, cosine may be approximated by its second-order Taylor expansion, and $x_{ij} \geq 4r_{ij}$. Thus, (22) provides an approximate relation between voltage angle difference and line losses.

C. Linearization of Radiation Heat Rate

When (19) is combined with an initial temperature $T^0_{\mathrm{l,C}}$ and (22), the resulting initial value problem should make it possible to determine conductor temperature $T_{\mathrm{l,C}}(t_n)$ at a later time t_n. We substitute (20)-(22) into (19) and attempt to solve for temperature:

$$\frac{dT}{dt} = \frac{1}{mC_p}\big[f^{\mathrm{loss}}_{ij} - \eta_c\left(T_{\mathrm{l,C}}(t) - T_{\mathrm{a,C}}\right) - \eta_r\left(T_{\mathrm{l,K}}(t)^4 - T^4_{\mathrm{a,K}}\right) + q_s\big] \quad (23)$$

If we suppose that power flow, ambient temperature, and solar heat rate are constant, this differential equation is still fourth-order in conductor temperature $T_{\mathrm{C}}(t)$ due to radiation. Fortunately, q_r is approximately linear over our temperature range of interest (from ambient temperature to temperature limit). We replace q_r by $\tilde{q}_r$, a conservative linearization:[9]

$$\tilde{q}_r = \eta_r\left(T^4_{\mathrm{m,K}} - T^4_{\mathrm{a,K}}\right) + 4\eta_r T^3_{\mathrm{m,K}}(T_{\mathrm{l,C}}(t) - T_{\mathrm{m,C}}), \quad (24)$$

where $T_{\mathrm{m,C}}$ is the average (midpoint between) ambient and conductor limit temperatures in Celsius, and $T_{\mathrm{m,K}}$ is $T_{\mathrm{m,C}}$ converted to Kelvin. After substitution of (24), the heat balance equation becomes linear in conductor temperature, and the IVP has a straightforward solution.

D. Line Temperature as Recursive Relationship

Substitution of (24) into (23) yields the approximate heat balance equation

$$\frac{dT_{\mathrm{l,C}}}{dt} = aT_{\mathrm{l,C}}(t) + b\ , \quad (25)$$

where constants a and b are defined as

$$a = \frac{1}{mC_p}\left[-\eta_c - 4\eta_r T^3_{\mathrm{m,K}}\right] \quad (26a)$$

$$b = \frac{1}{mC_p}\big[f^{\mathrm{loss}}_{ij} + \eta_c T_{\mathrm{a,C}} - \eta_r\left(T^4_{\mathrm{m,K}} - T^4_{\mathrm{a,K}}\right) + 4\eta_r T_{\mathrm{m,C}}\cdot T^3_{\mathrm{m,K}} + q_s\big] \quad (26b)$$

The IVP (25) has a straightforward solution:

$$T_{\mathrm{l,C}}(t) = ke^{at} - \frac{b}{a}, \quad (27)$$

where $k = T_{\mathrm{l,C}}(0) + b/a$. Note that b is influenced by power flow (via f^{loss}_{ij} according to (22)), but a is not.

The only variables in (27) are initial temperature and angle differences during each time interval. There is therefore a recursive relationship between final temperature and initial temperature that involves only angle differences. The derivation of this recursive relationship is an exercise in messy linear algebra; it is omitted here for brevity.

[9] Because a transmission line is hotter than surrounding air, radiation tends to decrease line temperature. Thus, a conservative approach will underestimate q_r. Plotting (24) shows that it does indeed underestimate q_r.

ACKNOWLEDGMENT

The authors would like to thank Dr. M. Chertkov and Dr. S. Backhaus of Los Alamos National Laboratory for discussions and notes that assisted in the transition from instantaneous to temporal settings, and Dr. D. Bienstock for his expertise and practical assistance in the solution of trust region subproblems.

REFERENCES

[1] J. Rogers, S. Fink, and K. Porter, "Examples of wind energy curtailment practices," 2010.

[2] B. Parsons, M. Milligan, B. Zavadil, D. Brooks, B. Kirby, K. Dragoon, and J. Caldwell, "Grid impacts of wind power: a summary of recent studies in the united states," *Wind Energy*, vol. 7, no. 2, pp. 87–108, 2004.

[3] M. Chertkov, F. Pan, and M. Stepanov, "Predicting failures in power grids: The case of static overloads," *IEEE Transactions on Smart Grid*, vol. 2, no. 1, pp. 162–172, Mar. 2011.

[4] M. Chertkov, M. Stepanov, F. Pan, and R. Baldick, "Exact and efficient algorithm to discover extreme stochastic events in wind generation over transmission power grids," in *Proc. 2011 50th IEEE Conference on Decision and Control and European Control Conference (CDC-ECC)*, 2011, pp. 2174–2180.

[5] S. Baghsorkhi and I. Hiskens, "Analysis tools for assessing the impact of wind power on weak grids," in *Proc. Systems Conference (SysCon), 2012 IEEE International*, 2012, pp. 1–8.

[6] C. Coffrin, P. Van Hentenryck, and R. Bent, "Approximating line losses and apparent power in AC power flow linearizations," pp. 1–8.

[7] H. Hijazi, C. Coffrin, and P. Van Hentenryck, "Convex quadratic relaxations of nonlinear programs in power systems," *Optimization Online*, 2013. [Online]. Available: http://www.optimization-online.org/DB_FILE/2013/09/4057.pdf

[8] C. Coffrin and P. Van Hentenryck, "A Linear-Programming Approximation of AC Power Flows," *INFORMS Journal on Computing*, vol. 26, no. 4, pp. 718–734, Nov. 2014. [Online]. Available: http://pubsonline.informs.org/doi/abs/10.1287/ijoc.2014.0594

[9] H. Banakar, N. Alguacil, and F. Galiana, "Electrothermal coordination part I: theory and implementation schemes," *IEEE Transactions on Power Systems*, vol. 20, no. 2, pp. 798–805, May 2005.

[10] J. Kersulis, I. Hiskens, M. Chertkov, S. Backhaus, and D. Bienstock, "Temperature-based instanton analysis: Identifying vulnerability in transmission networks," in *PowerTech, 2015 IEEE Eindhoven*, Jun. 2015, pp. 1–6.

[11] "IEEE Standard for Calculating the Current-Temperature Relationship of Bare Overhead Conductors," *IEEE Std 738-2012 (Revision of IEEE Std 738-2006 - Incorporates IEEE Std 738-2012 Cor 1-2013)*, pp. 1–72, Dec. 2013.

[12] M. Almassalkhi and I. Hiskens, "Model-predictive cascade mitigation in electric power systems with storage and renewables – part I: Theory and implementation," *IEEE Transactions on Power Systems*, vol. PP, no. 99, pp. 1–11, 2014.

[13] B. Hodge and M. Milligan, "Wind power forecasting error distributions over multiple timescales," in *2011 IEEE Power and Energy Society General Meeting*, Jul. 2011, pp. 1–8.

[14] J. Tastu, P. Pinson, and H. Madsen, "Space-time trajectories of wind power generation: Parameterized precision matrices under a Gaussian copula approach," in *Modeling and Stochastic Learning for Forecasting in High Dimensions*, ser. Lecture Notes in Statistics, X. Brossat, Ed. Springer, 2015, pp. 267–296.

[15] D. Bienstock and A. Michalka, "Polynomial Solvability of Variants of the Trust-region Subproblem," in *Proceedings of the Twenty-Fifth Annual ACM-SIAM Symposium on Discrete Algorithms*, ser. SODA '14. Portland, Oregon: SIAM, 2014, pp. 380–390. [Online]. Available: http://dl.acm.org/citation.cfm?id=2634074.2634102

[16] O. Mehanna, K. Huang, B. Gopalakrishnan, A. Konar, and N. Sidiropoulos, "Feasible point pursuit and successive approximation of non-convex QCQPs," *IEEE Signal Processing Letters*, vol. PP, no. 99, pp. 1–1, 2014.

[17] L. V. Foster and T. Davis, "Reliable calculation of numerical rank, null space bases, basic solutions and pseudoinverse solutions using suitesparseqr," in *Householder Symposium XVIII on Numerical Linear Algebra*, 2011, p. 79.

[18] H. Pandzic, Y. Dvorkin, T. Qiu, Y. Wang, and D. Kirschen. Unit Commitment under Uncertainty - GAMS Models, Library of the Renewable Energy Analysis Lab (REAL), University of Washington, Seattle, USA.

[19] M. Almassalkhi and I. Hiskens, "Model-predictive cascade mitigation in electric power systems with storage and renewables – part II: Case-study," vol. 30, no. 1, pp. 78–87.
[20] L. Freris and D. Infield, *Renewable energy in power systems*. John Wiley & Sons, 2008.
[21] R. D. Zimmerman, C. E. Murillo-Sánchez, and R. J. Thomas, "Matpower: Steady-state operations, planning, and analysis tools for power systems research and education," *Power Systems, IEEE Transactions on*, vol. 26, no. 1, pp. 12–19, 2011.

PLACE PHOTO HERE

Jonas Kersulis (S'12) received the B.S. degree in electrical engineering from the University of Missouri-St. Louis, St. Louis, MO USA; and the M.S. degree in Electrical Engineering:Systems from the University of Michigan, Ann Arbor, MI, USA, where he is currently working on his PhD.

His research interests include power system modeling and optimization.

Jonas is a member of the IEEE Power and Energy Society.

PLACE PHOTO HERE

Ian A. Hiskens (S'77–M'80–SM'96–F'06) received the B.Eng. degree in electrical engineering and the B.App.Sc. degree in mathematics from the Capricornia Institute of Advanced Education, Rockhampton, Australia, in 1980 and 1983 respectively, and the Ph.D. degree in electrical engineering from the University of Newcastle, Australia, in 1991.

He is the Vennema Professor of Engineering in the Department of Electrical Engineering and Computer Science, University of Michigan, Ann Arbor, MI, USA. He has held prior appointments in the Queensland electricity supply industry, and various universities in Australia and the United States. His research interests lie at the intersection of power system analysis and systems theory, with recent activity focused largely on integration of renewable generation and controllable loads.

Dr. Hiskens is actively involved in various IEEE societies, and is VP-Finance of the IEEE Systems Council. He is a Fellow of Engineers Australia, and a Chartered Professional Engineer in Australia.